SIAM J. NUMER. ANAL.
Vol. 46, No. 5, pp. 2443–2468

SEMI-IMPLICIT TIME-DISCRETIZATION SCHEMES FOR THE BIDOMAIN MODEL*

MARC ETHIER† AND YVES BOURGAULT‡

Abstract. The bidomain model is a system of partial differential equations used to model the propagation of electrical potential waves in the myocardium. It is composed of coupled parabolic and elliptic partial differential equations, as well as at least one ordinary differential equation to model the ion activity through the cardiac cell membranes. The purpose of this paper is to propose and analyze several implicit, semi-implicit, and explicit time-stepping methods to solve that model, in particular to avoid the expensive resolution of a nonlinear system through the Newton–Raphson method. We identify necessary stability conditions on the time step Δt for the proposed methods through a theoretical analysis based on energy estimates. We next compare the methods for one- and two-dimensional test cases, in terms of both stability and accuracy of the numerical solutions. The theoretical stability conditions are seen to be consistent with those observed in practice. Our analysis allows us to recommend using either the Crank–Nicolson/Adams–Bashforth method or the second order semi-implicit backward differention method. These semi-implicit methods produce a good numerical solution; unlike the explicit methods, their stability does not depend on the spatial grid size; and unlike the implicit methods, they do not require the resolution of a system of nonlinear equations.

Key words. bidomain model, electrophysiology, finite elements, time-stepping schemes, stability analysis

AMS subject classifications. 65M60, 65M12, 65F10

DOI. 10.1137/070680503

1. Introduction.

The bidomain model is used in electrophysiology to model the propagation of electrical potential waves in the myocardium. It is obtained by homogenization over the discrete cells of the myocardium, in particular using the regular arrangement of these in fibers [7, 14]. At each point in the computational domain, two electrical potentials, namely, the intracellular potential u_i and the extracellular potential u_e, are recovered, representing the average of the electrical potential over the extracellular and the intracellular space, respectively, in the vicinity of that point.

There are many ways to write the bidomain model's equations. Many of them are introduced in [11], where their respective merits are also discussed. We will use the following formulation:

$$\frac{\partial u}{\partial t} = \frac{1}{\epsilon} f(u,v) + \nabla \cdot (\sigma_i \nabla u) + \nabla \cdot (\sigma_i \nabla u_e)\,, \tag{1.1}$$

$$\nabla \cdot (\sigma_i \nabla u + (\sigma_i + \sigma_e)\nabla u_e) = 0, \tag{1.2}$$

$$\frac{\partial v}{\partial t} = \epsilon g(u,v), \tag{1.3}$$

where $u = u_i - u_e$ is the action or transmembrane potential, σ_i and σ_e are second order tensors representing, respectively, the intracellular and the extracellular tissue's

*Received by the editors January 19, 2007; accepted for publication (in revised form) January 25, 2008; published electronically June 11, 2008. This work was partly supported by an NSERC scholarship and an NSERC operating grant.
http://www.siam.org/journals/sinum/46-5/68050.html
†Department of Mathematics and Statistics, University of Ottawa, Ottawa, ON, K1N 6N5, Canada (marcdethier@gmail.com).
‡Corresponding author. Department of Mathematics and Statistics, University of Ottawa, Ottawa, ON, K1N 6N5, Canada (ybourg@uottawa.ca).

electrical conductivity in each spatial direction, v is a lumped ionic variable, and ϵ is a parameter linked to the ratio between the repolarization rate and the tissue excitation rate [21]. It has been proved that the bidomain model has a unique solution [4, 7]. In [7] the bidomain model is formulated as a system of degenerate parabolic inequalities, while in [4] the analysis is based on the more standard theory of nonlinear parabolic PDEs. We chose to use this last formulation of the bidomain model as the basis of our numerical method because of its connection with standard parabolic and elliptic PDEs where the theory of finite element methods is well developed. We refer to [11, 19] for a more complete discussion on the different formulations of the bidomain model and their use in numerical simulations.

The equation (1.3) is not properly part of the bidomain model but rather models the ionic activity across the cellular membrane, responsible for the electrical activation of the tissue. Several models may be used for this task, the most widely known being the Hodgkin–Huxley model, originally introduced for the propagation of nerve influx inside neurons. Other models more adapted to the heart muscle have been derived, such as the Noble and Luo–Rudy models [14]. We will use the FitzHugh–Nagumo equations, which are a simplification of the Hodgkin–Huxley equations. We can therefore write the functions f and g as

$$f(u,v) = u - \frac{u^3}{3} - v, \tag{1.4}$$

$$g(u,v) = u + \beta - \gamma v, \tag{1.5}$$

where γ is a parameter controlling the ion transport and β is linked to cell excitability.

After an appropriate discretization in space, (1.1)–(1.3) read as a system of algebraic-differential equations, simply because the second equation (1.2) comes with no time derivative. The choice of a time-stepping method for that system of algebraic-differential equations has a strong impact on the stability, computational time, memory use, and quality of the numerical solution. Until recently, the numerical resolution of the bidomain model by low order explicit time-stepping methods had been very popular [11, 18, 22]. Explicit methods are easy to program and inexpensive in terms of memory use. Each time step costs typically little in terms of computational time with these methods. On the other hand, they suffer from strong limitations on the time step Δt to ensure the stability of the solution. Therefore, some of the efforts for solving the bidomain model migrated towards fully implicit [5, 11, 17], semi-implicit [9, 11, 13, 19], and operator-splitting [15, 16, 25, 26] methods. Implicit methods have much weaker conditions on the time step for their stability, but if the system to solve is nonlinear, as is the bidomain model with any ion kinetics, they require the solution of a large system of nonlinear equations at every time step. Semi-implicit methods—also called semi-explicit or implicit-explicit (IMEX)—combine explicit and implicit methods: they solve the linear terms implicitly and the nonlinear terms explicitly [1, 2, 23]. These methods are more stable than explicit methods but less so than implicit methods, and, while they require the solution of a system of equations at every time step, it is a system of linear equations.

So far, the semi-implicit methods used for the bidomain model have been only first order in time [9, 11, 13, 19], even if some of these rest on a splitting of the second order terms according to the Crank–Nicolson scheme. This is simply due to the fact that the ionic currents in the first equation (1.1) are taken explicitly as for the forward Euler scheme, lowering the global order of these semi-implicit methods. In [1, 2, 23], higher order semi-implicit schemes are proposed and analyzed. The goal of this paper

is precisely to study the use of these higher order semi-implicit schemes to solve the bidomain model.

The paper is organized as follows: we will introduce several time-stepping schemes in section 2 and then exhibit theoretical stability conditions on the time step in section 3. This will require an extension of the usual stability estimates for such semi-implicit schemes, such as done in [1], because the bidomain model can be rewritten as a system of nonlinear reaction-diffusion equations (see [4] for details) but is not solved as a standard reaction-diffusion equation. Indeed, the elliptic equation (1.2) is solved at each time step. We will obtain theoretical stability conditions showing the necessity of taking implicitly a portion of the second order terms in u and u_e, for time-stepping methods of all orders, to avoid time steps in $O(h^2)$. In section 4, numerical results will be shown with an emphasis on the stability and accuracy of the proposed schemes.

2. Numerical methods. The goal of this section is to introduce the different numerical methods studied in this article.

2.1. Space discretization. We first introduce a spatial semidiscretization of the bidomain model through first order simplicial Lagrange finite elements. Let us assume that the domain Ω can be covered by a regular partition $\mathscr{T}$ of simplexes—edges in one dimension, triangles in two dimensions, and tetrahedra in three dimensions—of maximal diameter h, with $N+1$ nodes, noted x_0 to x_N. Consider the space P_h^1 of continuous linear finite elements on $\mathscr{T}$ and the usual basis of hat functions $\Phi_0^h, \dots, \Phi_N^h$ attached to the nodes $x_0, \dots, x_N$, respectively. Here we suppose that homogeneous Neumann boundary conditions are used on $\partial\Omega$ for both u and u_e.

The semidiscrete bidomain problem then reads as: find a $[u, u_e, v] \in \mathscr{C}([0,T]; P_h^1)^3$ solution of the following variational equations:

$$\int_\Omega u_t \Phi_j^h \,\mathrm{d}\mathbf{x} = \frac{1}{\epsilon}\int_\Omega f(u,v)\Phi_j^h \,\mathrm{d}\mathbf{x} - \int_\Omega (\sigma_i \nabla(u+u_e))\cdot\nabla\Phi_j^h \,\mathrm{d}\mathbf{x}, \tag{2.1}$$

$$\int_\Omega (\sigma_i \nabla u)\cdot\nabla\Phi_j^h \,\mathrm{d}\mathbf{x} + \int_\Omega ((\sigma_i+\sigma_e)\nabla u_e)\cdot\nabla\Phi_j^h \,\mathrm{d}\mathbf{x} = 0, \tag{2.2}$$

$$\int_\Omega v_t \Phi_j^h \,\mathrm{d}\mathbf{x} = \epsilon\int_\Omega g(u,v)\Phi_j^h \,\mathrm{d}\mathbf{x} \tag{2.3}$$

for all $j = 0, \dots, N$.

By setting $u(t) = \sum_{i=0}^N u_i\Phi_i^h$, $u_e(t) = \sum_{i=0}^N u_{e,i}\Phi_i^h$, and $v(t) = \sum_{i=0}^N v_i\Phi_i^h$, we can rewrite these equations under matrix form:

$$M\mathbf{u}_t = \frac{1}{\epsilon}F(\mathbf{u},\mathbf{v}) - A_i(\mathbf{u}+\mathbf{u_e}), \tag{2.4}$$

$$A_i\mathbf{u} + (A_i+A_e)\mathbf{u_e} = \mathbf{0}, \tag{2.5}$$

$$M\mathbf{v}_t = \epsilon\, G(\mathbf{u},\mathbf{v}), \tag{2.6}$$

where $\mathbf{u} = [u_0, \dots, u_N]^T$, $\mathbf{u_e} = [u_{e,0}, \dots, u_{e,N}]^T$, $\mathbf{v} = [v_0, \dots, v_N]^T$, A_i and A_e are stiffness matrices obtained by integrating the second order terms, including, respectively, the tensors σ_i and σ_e, M is the mass matrix such that $M(i,j) = \int_\Omega \Phi_i^h\Phi_j^h \,\mathrm{d}\mathbf{x}$, and F and G are operators obtained by the integration of the zeroth order terms. For example, by using mass lumping to simplify the nonlinear operator F, we can define G and F as

$$G(\mathbf{u},\mathbf{v}) = M(\mathbf{u}-\gamma\mathbf{v}) + \beta\left[\int_\Omega \Phi_0^h \,\mathrm{d}\mathbf{x}, \dots, \int_\Omega \Phi_N^h \,\mathrm{d}\mathbf{x}\right]^T$$

and

$$F(\mathbf{u},\mathbf{v}) = M\left(\mathbf{u} - \frac{\mathbf{u^3}}{3} - \mathbf{v}\right),$$

where $\mathbf{u^3} = [u_0^3, \ldots, u_N^3]^T$.

2.2. Time discretization. We have considered a variety of explicit, implicit, and IMEX finite difference methods, using a constant time step Δt, for the time discretization. Note that the presence of (2.5) in the system has the effect that it is necessary to solve a system of equations at every time step, even for usually completely explicit methods such as the forward Euler scheme. Therefore, the following equation is part of every one of our time-discretization schemes:

$$A_i \mathbf{u^{n+1}} + (A_i + A_e)\mathbf{u_e^{n+1}} = \mathbf{0}.$$

That equation will not be repeated below, but it is understood that it is always part of the resulting fully discrete bidomain problem. We now present all of the schemes.

2.2.1. First order methods.

(i) forward Euler:

$$M\frac{\mathbf{u^{n+1}} - \mathbf{u^n}}{\Delta t} = \frac{1}{\epsilon}F\left(\mathbf{u^n}, \mathbf{v^n}\right) - A_i\left(\mathbf{u^n} + \mathbf{u_e^n}\right), \tag{2.7}$$
$$M\frac{\mathbf{v^{n+1}} - \mathbf{v^n}}{\Delta t} = \epsilon G\left(\mathbf{u^n}, \mathbf{v^n}\right).$$

(ii) forward-backward Euler:

$$M\frac{\mathbf{u^{n+1}} - \mathbf{u^n}}{\Delta t} = \frac{1}{\epsilon}F\left(\mathbf{u^n}, \mathbf{v^n}\right) - A_i\left(\mathbf{u^{n+1}} + \mathbf{u_e^{n+1}}\right), \tag{2.8}$$
$$M\frac{\mathbf{v^{n+1}} - \mathbf{v^n}}{\Delta t} = \epsilon G\left(\mathbf{u^n}, \mathbf{v^n}\right).$$

(iii) Crank–Nicolson–forward Euler (Crank–Nicolson (CN)):

$$M\frac{\mathbf{u^{n+1}} - \mathbf{u^n}}{\Delta t} = \frac{1}{\epsilon}F\left(\mathbf{u^n}, \mathbf{v^n}\right) - \frac{1}{2}A_i\left(\mathbf{u^{n+1}} + \mathbf{u_e^{n+1}}\right) - \frac{1}{2}A_i\left(\mathbf{u^n} + \mathbf{u_e^n}\right), \tag{2.9}$$
$$M\frac{\mathbf{v^{n+1}} - \mathbf{v^n}}{\Delta t} = \epsilon G\left(\mathbf{u^n}, \mathbf{v^n}\right).$$

(iv) IMEX first order Gear:

$$M\frac{\frac{3}{2}\mathbf{u^{n+1}} - 2\mathbf{u^n} + \frac{1}{2}\mathbf{u^{n-1}}}{\Delta t} = \frac{1}{\epsilon}F\left(\mathbf{u^n}, \mathbf{v^n}\right) - A_i\left(\mathbf{u^{n+1}} + \mathbf{u_e^{n+1}}\right), \tag{2.10}$$
$$M\frac{\frac{3}{2}\mathbf{v^{n+1}} - 2\mathbf{v^n} + \frac{1}{2}\mathbf{v^{n-1}}}{\Delta t} = \epsilon G\left(\mathbf{u^{n+1}}, \mathbf{v^{n+1}}\right).$$

(v) backward Euler:

$$M\frac{\mathbf{u^{n+1}} - \mathbf{u^n}}{\Delta t} = \frac{1}{\epsilon}F\left(\mathbf{u^{n+1}}, \mathbf{v^{n+1}}\right) - A_i\left(\mathbf{u^{n+1}} + \mathbf{u_e^{n+1}}\right), \tag{2.11}$$
$$M\frac{\mathbf{v^{n+1}} - \mathbf{v^n}}{\Delta t} = \epsilon G\left(\mathbf{u^{n+1}}, \mathbf{v^{n+1}}\right).$$

2.2.2. Second order methods.

(i) Crank–Nicolson/Adams–Bashforth (CNAB):

$$\begin{aligned} M\frac{\mathbf{u^{n+1}}-\mathbf{u^n}}{\Delta t} &= \frac{1}{\epsilon}\left(\frac{3}{2}F\left(\mathbf{u^n},\mathbf{v^n}\right)-\frac{1}{2}F\left(\mathbf{u^{n-1}},\mathbf{v^{n-1}}\right)\right) \\ &\quad -\frac{1}{2}A_i\left(\mathbf{u^{n+1}}+\mathbf{u_e^{n+1}}\right)-\frac{1}{2}A_i\left(\mathbf{u^n}+\mathbf{u_e^n}\right), \\ M\frac{\mathbf{v^{n+1}}-\mathbf{v^n}}{\Delta t} &= \epsilon\left(\frac{3}{2}G\left(\mathbf{u^n},\mathbf{v^n}\right)-\frac{1}{2}G\left(\mathbf{u^{n-1}},\mathbf{v^{n-1}}\right)\right). \end{aligned} \tag{2.12}$$

(ii) modified Crank–Nicolson/Adams–Bashforth (MCNAB):

$$\begin{aligned} M\frac{\mathbf{u^{n+1}}-\mathbf{u^n}}{\Delta t} &= \frac{1}{\epsilon}\left(\frac{3}{2}F\left(\mathbf{u^n},\mathbf{v^n}\right)-\frac{1}{2}F\left(\mathbf{u^{n-1}},\mathbf{v^{n-1}}\right)\right)-\frac{9}{16}A_i\left(\mathbf{u^{n+1}}+\mathbf{u_e^{n+1}}\right) \\ &\quad -\frac{3}{8}A_i\left(\mathbf{u^n}+\mathbf{u_e^n}\right)-\frac{1}{16}A_i\left(\mathbf{u^{n-1}}+\mathbf{u_e^{n-1}}\right), \\ M\frac{\mathbf{v^{n+1}}-\mathbf{v^n}}{\Delta t} &= \epsilon\left(\frac{3}{2}G\left(\mathbf{u^n},\mathbf{v^n}\right)-\frac{1}{2}G\left(\mathbf{u^{n-1}},\mathbf{v^{n-1}}\right)\right). \end{aligned} \tag{2.13}$$

(iii) second order semi-implicit backward differentiation (SBDF):

$$\begin{aligned} M\frac{\frac{3}{2}\mathbf{u^{n+1}}-2\mathbf{u^n}+\frac{1}{2}\mathbf{u^{n-1}}}{\Delta t} &= \frac{1}{\epsilon}\left(2F\left(\mathbf{u^n},\mathbf{v^n}\right)-F\left(\mathbf{u^{n-1}},\mathbf{v^{n-1}}\right)\right) \\ &\quad -A_i\left(\mathbf{u^{n+1}}+\mathbf{u_e^{n+1}}\right), \\ M\frac{\frac{3}{2}\mathbf{v^{n+1}}-2\mathbf{v^n}+\frac{1}{2}\mathbf{v^{n-1}}}{\Delta t} &= \epsilon\left(2G\left(\mathbf{u^n},\mathbf{v^n}\right)-G\left(\mathbf{u^{n-1}},\mathbf{v^{n-1}}\right)\right). \end{aligned} \tag{2.14}$$

(iv) implicit Gear:

$$\begin{aligned} M\frac{\frac{3}{2}\mathbf{u^{n+1}}-2\mathbf{u^n}+\frac{1}{2}\mathbf{u^{n-1}}}{\Delta t} &= \frac{1}{\epsilon}F\left(\mathbf{u^{n+1}},\mathbf{v^{n+1}}\right)-A_i\left(\mathbf{u^{n+1}}+\mathbf{u_e^{n+1}}\right), \\ M\frac{\frac{3}{2}\mathbf{v^{n+1}}-2\mathbf{v^n}+\frac{1}{2}\mathbf{v^{n-1}}}{\Delta t} &= \epsilon G\left(\mathbf{u^{n+1}},\mathbf{v^{n+1}}\right). \end{aligned} \tag{2.15}$$

2.2.3. Third order method. Third order SBDF:

$$\begin{aligned} M\frac{\frac{11}{6}\mathbf{u^{n+1}}-3\mathbf{u^n}+\frac{3}{2}\mathbf{u^{n-1}}-\frac{1}{3}\mathbf{u^{n-2}}}{\Delta t} &= \frac{1}{\epsilon}\big(3F\left(\mathbf{u^n},\mathbf{v^n}\right)-3F\left(\mathbf{u^{n-1}},\mathbf{v^{n-1}}\right) \\ &\quad +F\left(\mathbf{u^{n-2}},\mathbf{v^{n-2}}\right)\big)-A_i\left(\mathbf{u^{n+1}}+\mathbf{u_e^{n+1}}\right), \\ M\frac{\frac{11}{6}\mathbf{v^{n+1}}-3\mathbf{v^n}+\frac{3}{2}\mathbf{v^{n-1}}-\frac{1}{3}\mathbf{v^{n-2}}}{\Delta t} &= \epsilon\big(3G\left(\mathbf{u^n},\mathbf{v^n}\right)-3G\left(\mathbf{u^{n-1}},\mathbf{v^{n-1}}\right) \\ &\quad +G\left(\mathbf{u^{n-2}},\mathbf{v^{n-2}}\right)\big). \end{aligned} \tag{2.16}$$

By looking at (2.1)–(2.3), one can see that u_e appears in these equations only in the form of its gradient. Because of the Neumann boundary conditions, the variable u_e can be determined only modulo a constant. In other words, the numerical schemes

(2.7)–(2.16) give rise to singular systems of equations. There exist many ways to solve this problem [3]; we chose to fix u_e at a specific value on a particular node for every time step. Note that the indefiniteness on u is naturally removed by the nonlinear term in f in the first equation of the bidomain model. See [4] for details on that indefiniteness of the system, its physical significance, and its mathematical treatment for the continuous problem.

Even after removing the indefiniteness, the resulting linear systems are still very ill conditioned. The choice of linear solver is therefore hard. In the one-dimensional (1D) case, it is possible to use a direct solver such as the LU factorization. Because of memory constraints, this becomes much less possible in higher dimensions. Using an iterative method [10, 24] becomes necessary. Our numerical tests have convinced us that the conjugate gradient method is most appropriate in this case. We have also used the incomplete LU factorization to precondition the system. Our computer memory constraints drive the level of fill we may use with this preconditioner: in 2D with moderately fine meshes, we have been able to use two levels of fill, but finer meshes, as well as 3D meshes, would probably require us to use only one level of fill or none at all.

3. Numerical analysis of the schemes. This section is dedicated to demonstrating that the previously seen numerical schemes remain stable under appropriate conditions on the time step Δt. We also analyze the semidiscrete problem introduced in section 2.1 and prove that its solution is unconditionally stable.

In the rest of the paper, $\|\cdot\|_0$ refers to the L^2 norm over Ω and $|\cdot|_1$ to the H^1 seminorm over Ω. The constants m_i and m_e denote the infimum of the eigenvalues of σ_i and σ_e, respectively, and M_i and M_e the supremum of these eigenvalues, with the infimum and supremum taken all over Ω as well.

3.1. Stability of the semidiscrete method. We analyze the semidiscrete formulation (2.1)–(2.3) of the bidomain model. We first redefine the function g as $g(u,v) = u - \gamma v$ and set $S = \epsilon\beta$. This ensures that the graph of f and g goes through the origin. The term S then goes into the right-hand side of the PDE.

By using as test functions $\Phi_j^h = u(t)$, $u_e(t)$, and $v(t)$ in (2.1), (2.2), and (2.3), respectively, adding the three equations so obtained, and using the following lower bound for the diffusive terms:

$$\begin{aligned}\int_\Omega (\sigma_i\nabla(u+u_e))\cdot\nabla(u+u_e)\,\mathrm{d}\mathbf{x} + \int_\Omega (\sigma_e\nabla u_e)\cdot\nabla u_e\,\mathrm{d}\mathbf{x} &\geq m_i|u+u_e|_1^2 + m_e|u_e|_1^2 \\ &\geq \bar{m}(|u|_1^2 + |u_e|_1^2),\end{aligned} \tag{3.1}$$

where $\bar{m}$ depends on m_i and m_e by equivalence of seminorms, one easily obtains the following inequalities:

$$\begin{aligned}&\frac{d}{dt}\left[\|u\|_0^2 + \|v\|_0^2\right] + 2\bar{m}\left(|u|_1^2 + |u_e|_1^2\right) \\ &\qquad\leq \frac{2}{\epsilon}\left(\int_\Omega u^2\,\mathrm{d}\mathbf{x} - \frac{1}{3}\int_\Omega u^4\,\mathrm{d}\mathbf{x} - \int_\Omega uv\,\mathrm{d}\mathbf{x}\right) \\ &\qquad\quad + 2\epsilon\left(\int_\Omega uv\,\mathrm{d}\mathbf{x} - \gamma\int_\Omega v^2\,\mathrm{d}\mathbf{x}\right) + 2\int_\Omega Sv\,\mathrm{d}\mathbf{x} \\ &\qquad\leq \frac{2}{\epsilon}\|u\|_0^2 - 2\epsilon\gamma\|v\|_0^2 + \frac{\left|\frac{1}{\epsilon}-\epsilon\right|}{k}\|u\|_0^2 + \left|\frac{1}{\epsilon}-\epsilon\right| k\|v\|_0^2 + \frac{1}{r}\|S\|_0^2 + r\|v\|_0^2 \\ &\qquad\leq C_1\left[\|u\|_0^2 + \|v\|_0^2\right] + C_2\|S\|_0^2,\end{aligned} \tag{3.2}$$

where the constants k, $r > 0$, $C_1 = \max\{2/\epsilon + |1/\epsilon - \epsilon|/k, |1/\epsilon - \epsilon|k + r - 2\epsilon\gamma\}$, and $C_2 = 1/r$, owing to the fact that, for $a, b \in \mathbb{R}$ and for $k > 0$, $ab \le a^2/2k + b^2k/2$.

Applying Gronwall's lemma [8, Lemma 6.9, p. 284] to the inequality (3.2) gives:

$$\|u(t)\|_0^2 + \|v(t)\|_0^2 \le e^{C_1 t}\left[\|u(0)\|_0^2 + \|v(0)\|_0^2\right] + \int_0^t e^{C_1(t-\tau)}\left[C_2\|S\|_0^2 - 2\bar{m}\left(|u|_1^2 + |u_e|_1^2\right)\right]\mathrm{d}\tau \tag{3.3}$$

$$\Rightarrow \max_{t\in[0,T]}\left[\|u(t)\|_0^2 + \|v(t)\|_0^2\right] \le e^{C_1 T}\left[\|u_0\|_0^2 + \|v_0\|_0^2\right] + C_2\int_0^T e^{C_1(T-\tau)}\|S\|_0^2\,\mathrm{d}\tau,$$

where u_0 and $v_0 \in P_h^1$ are the initial data for the semidiscrete formulation. In other words, u and v remain bounded in $L^\infty(0,T;L^2(\Omega))$.

From (3.3), we obtain

$$2\bar{m}\int_0^T e^{C_1(T-\tau)}\left(|u|_1^2 + |u_e|_1^2\right)\mathrm{d}\tau \le e^{C_1 T}\left[\|u_0\|_0^2 + \|v_0\|_0^2\right] + C_2\int_0^T e^{C_1(T-\tau)}\|S\|_0^2\,\mathrm{d}\tau$$

$$\Rightarrow \int_0^T \left(|u|_1^2 + |u_e|_1^2\right)\mathrm{d}\tau \le \frac{e^{C_1 T}}{2\bar{m}}\left[\|u_0\|_0^2 + \|v_0\|_0^2\right] + \frac{C_2}{2\bar{m}}\int_0^T e^{C_1(T-\tau)}\|S\|_0^2\,\mathrm{d}\tau. \tag{3.4}$$

This shows that the $H^1(\Omega)$ seminorm of u and u_e remains L^2 bounded on any interval $[0,T]$.

By putting together the bounds obtained above, we find that the solution of the semidiscrete problem remains bounded in the following spaces:

$$\begin{aligned} &u \in L^\infty(0,T;L^2(\Omega)) \cap L^2(0,T;H^1(\Omega)),\\ &u_e \in L^2(0,T;H^1(\Omega)/\mathbb{R}),\\ &v \in L^\infty(0,T;L^2(\Omega)). \end{aligned} \tag{3.5}$$

In particular, the extracellular potential u_e is bounded only in $L^2(0,T;H^1(\Omega)/\mathbb{R})$, not in any $L^p(0,T;L^2(\Omega))$, since we can determine u_e only up to a constant. It is important to note that the relations (3.5) make use of the fact that the FitzHugh–Nagumo model is used for the ion activity. A nice feature is that the constants in the estimates (3.5) are independent from the cell size h of the space discretization. The semidiscrete problem is unconditionally stable. This is a main argument behind the existence proof given in [4].

3.2. Stability of the discrete methods. Let us now investigate the stability of some of the fully discrete numerical schemes introduced in section 2. We keep track as much as we can of the constants in the stability estimates to be able to identify the relevant parameters in the bidomain model controlling the stability of the numerical schemes.

3.2.1. Backward Euler. We consider the backward Euler method (2.11) as a representative of the implicit methods we have used. By using as test function Φ the

solutions u^{n+1}, u_e^{n+1}, and v^{n+1} in their respective variational equations, we obtain:

$$\int_\Omega \left[\frac{u^{n+1}-u^n}{\Delta t} - \frac{1}{\epsilon} f(u^{n+1}, v^{n+1})\right] u^{n+1}\,\mathrm{d}\mathbf{x} + \int_\Omega \left(\sigma_i \nabla (u^{n+1} + u_e^{n+1})\right) \cdot \nabla u^{n+1}\,\mathrm{d}\mathbf{x} = 0,$$

$$\int_\Omega (\sigma_i \nabla u^{n+1}) \cdot \nabla u_e^{n+1}\,\mathrm{d}\mathbf{x} + \int_\Omega \left((\sigma_i + \sigma_e)\nabla u_e^{n+1}\right) \cdot \nabla u_e^{n+1}\,\mathrm{d}\mathbf{x} = 0,$$

$$\int_\Omega \left[\frac{v^{n+1}-v^n}{\Delta t} - \epsilon g(u^{n+1}, v^{n+1})\right] v^{n+1}\,\mathrm{d}\mathbf{x} = \int_\Omega S^n v^{n+1}\,\mathrm{d}\mathbf{x}. \tag{3.6}$$

By adding these three equations, using the identity

$$2(a^{n+1}-a^n)a^{n+1} = (a^{n+1})^2 + (a^{n+1}-a^n)^2 - (a^n)^2,$$

and proceeding as for the semidiscrete method, we get:

$$\begin{aligned} &\|u^{n+1}\|_0^2 + \|u^{n+1}-u^n\|_0^2 - \|u^n\|_0^2 + \|v^{n+1}\|_0^2 + \|v^{n+1}-v^n\|_0^2 - \|v^n\|_0^2 \\ &\qquad + 2\Delta t\,\bar{m}\left(|u^{n+1}|_1^2 + |u_e^{n+1}|_1^2\right) \\ &\qquad \le \Delta t\, C_1 \left[\|u^{n+1}\|_0^2 + \|v^{n+1}\|_0^2\right] + \Delta t\, C_2 \|S^n\|_0^2, \end{aligned} \tag{3.7}$$

where C_1 and C_2 are defined as they were in the semidiscrete case. Now denote by M the index of the final time step (i.e., $T = M\Delta t$), and sum the previous inequality for n going from 0 to $m-1$, $1 \le m \le M$, to obtain:

$$\begin{aligned} &(1-\Delta t\, C_1)\left[\|u^m\|_0^2 + \|v^m\|_0^2\right] + 2\Delta t\bar{m} \sum_{n=1}^{m} \left(|u^n|_1^2 + |u_e^n|_1^2\right) \\ &\qquad \le \|u^0\|_0^2 + \|v^0\|_0^2 + \Delta t\, C_1 \sum_{n=0}^{m-1} \left[\|u^n\|_0^2 + \|v^n\|_0^2\right] + \Delta t\, C_2 \sum_{n=0}^{m-1} \|S^n\|_0^2. \end{aligned} \tag{3.8}$$

Now, from the discrete Gronwall lemma [20, Lemma 1.4.2, p. 14], by assuming that $\Delta t < 1/C_1$, it can be concluded that

$$\begin{aligned} \max_{n=1,\ldots,M} \left\{\|u^n\|_0^2 + \|v^n\|_0^2\right\} \le \Bigg(&\frac{1}{1-\Delta t\, C_1}\left[\|u^0\|_0^2 + \|v^0\|_0^2\right] \\ &+ \frac{C_2}{1-\Delta t\, C_1} \sum_{n=0}^{M-1} \Delta t\, \|S^n\|_0^2\Bigg) e^{\frac{TC_1}{1-\Delta t C_1}}. \end{aligned} \tag{3.9}$$

Let us extend the numerical solutions at discrete times t_n to functions u and v piecewise constant in time and such that $u(n\Delta t) = u^n, v(n\Delta t) = v^n$ for $n = 0, \ldots, M-1$. The last inequality means that $u, v \in L^\infty(0,T;L^2(\Omega))$. This property is true as long as $\sum_{n=0}^{M-1} \Delta t \|S^n\|_0^2$ remains bounded, which holds if $S \in L^2(0,T;L^2(\Omega))$.

Now return to (3.8). We can use that inequality to bound the other left-hand term:

$$\begin{aligned} \sum_{n=1}^{M} \Delta t \left(|u^n|_1^2 + |u_e^n|_1^2\right) \le &\frac{1}{2\bar{m}} \left(\|u^0\|_0^2 + \|v^0\|_0^2\right) + \frac{TC_1}{2\bar{m}} \max_n \left\{\|u^n\|_0^2 + \|v^n\|_0^2\right\} \\ &+ \frac{C_2}{2\bar{m}} \sum_{n=0}^{M-1} \Delta t\, \|S^n\|_0^2. \end{aligned} \tag{3.10}$$

The left-hand term in this last inequality is nothing more—extending the solution u and u_e to piecewise functions as before—than the $L^2(0,T)$ norm of $|u|_1$ and $|u_e|_1$. We can thus conclude that the solutions u, u_e, and v of the fully discrete backward Euler method live in the same functional spaces as in the semidiscrete case. The difference is that we have here a constraint on the time step Δt. To ensure the stability of the method, we must have $\Delta t < 1/C_1$. Since $C_1 = O(1/\epsilon)$ for $\epsilon \ll 1$, the stability of the backward Euler scheme is guaranteed for $\Delta t = O(\epsilon)$. Note that this condition is independent of h. The parameter ϵ controls the thickness of the depolarization/repolarization fronts, meaning that the time step Δt must be small enough to resolve that front to ensure stability.

3.2.2. Second order SBDF. We shall now consider the stability of the second order SBDF method (2.14). With u^{n+1}, u_e^{n+1}, and v^{n+1} as test functions, the associated variational equations read as follows:

$$\begin{aligned}
&\int_\Omega \left[\frac{3u^{n+1}-4u^n+u^{n-1}}{2\Delta t} - \frac{1}{\epsilon}\left(2f(u^n,v^n)-f(u^{n-1},v^{n-1})\right)\right]u^{n+1}\,\mathrm{d}\mathbf{x} \\
&\qquad + \int_\Omega \left(\sigma_i\nabla(u^{n+1}+u_e^{n+1})\right)\cdot\nabla u^{n+1}\,\mathrm{d}\mathbf{x} = 0, \\
&\int_\Omega (\sigma_i\nabla u^{n+1})\cdot\nabla u_e^{n+1}\,\mathrm{d}\mathbf{x} + \int_\Omega \left((\sigma_i+\sigma_e)\nabla u_e^{n+1}\right)\cdot\nabla u_e^{n+1}\,\mathrm{d}\mathbf{x} = 0, \\
&\int_\Omega \left[\frac{3v^{n+1}-4v^n+v^{n-1}}{2\Delta t} - \epsilon\left(2g(u^n,v^n)-g(u^{n-1},v^{n-1})\right)\right]v^{n+1}\,\mathrm{d}\mathbf{x} \\
&\qquad = \int_\Omega S^n v^{n+1}\,\mathrm{d}\mathbf{x}.
\end{aligned} \tag{3.11}$$

Since the reaction terms are taken explicitly, a milder dependency of the reaction terms on the variables u and v must be assumed; e.g., we suppose that f and g satisfy the following Lipschitz condition:

$$\begin{aligned}
\|f(u,v)\|_0 &\le L_f\left[\|u\|_0+\|v\|_0\right], \\
\|g(u,v)\|_0 &\le L_g\left[\|u\|_0+\|v\|_0\right],
\end{aligned} \tag{3.12}$$

where L_f, $L_g > 0$.

Remark 3.1. The functions $f(u,v) = u - \frac{u^3}{3} - v$ and $g(u,v) = u - \gamma v$ in the FitzHugh–Nagumo ionic model are not Lipschitzian. However, if we make the hypothesis that $u \in L^\infty(\Omega)$ and that there exists a constant $\mathscr{C} > 0$ such that $\|u\|_\infty \le \mathscr{C}$ for all time $t \in [0,T]$, we have

$$\begin{aligned}
\|f(u,v)\|_0 \le \|u\|_0 + \frac{1}{3}\|u^3\|_0 + \|v\|_0 &\le \|u\|_0 + \frac{1}{3}\|u\|_\infty^2\|u\|_0 + \|v\|_0 \\
&\le \left(\frac{\mathscr{C}^2}{3}+1\right)\|u\|_0 + \|v\|_0 \\
&\le L_f\left[\|u\|_0+\|v\|_0\right],
\end{aligned}$$

where $L_f = \frac{\mathscr{C}^2}{3}+1$. We can also bound the function g:

$$\|g(u,v)\|_0 \le \|u\|_0 + \gamma\|v\|_0 \le L_g\left[\|u\|_0+\|v\|_0\right],$$

where $L_g = \max\{1,\gamma\}$. We do observe numerically that, provided that the initial solution $(u_0(x), v_0(x))$ at all points $x \in \Omega$ is in a properly chosen box in the (u,v)-plane,

$(u(x,t), v(x,t))$ remains in that box for all time. In other words, u remains bounded in $L^\infty(\Omega)$, and the constants L_f and L_g can be practically identified. Basically it would mean that we can replace the cubic function f of the FitzHugh–Nagumo model by an affine function $\tilde{f}$ outside of that box without changing the solution, the function $\tilde{f}$ now being Lipschitzian. It should be noted though that, as far as we know, such a maximum principle has not been proven for the bidomain model with FitzHugh–Nagumo ion kinetics.

By adding the equations of system (3.11) and applying the identity

$$\begin{aligned}(6a^{n+1} - 8a^n + 2a^{n-1})a^{n+1} = (a^{n+1})^2 + (2a^{n+1} - a^n)^2 + (\delta_{tt}a^{n+1})^2 \\ - (a^n)^2 - (2a^n - a^{n-1})^2,\end{aligned}$$

where $\delta_{tt}a^{n+1} = a^{n+1} - 2a^n + a^{n-1}$ to the time-discretization term, we obtain

$$\begin{aligned}&\|u^{n+1}\|_0^2 + \|2u^{n+1} - u^n\|_0^2 - \|u^n\|_0^2 - \|2u^n - u^{n-1}\|_0^2 + \|v^{n+1}\|_0^2 \\ &\quad + \|2v^{n+1} - v^n\|_0^2 - \|v^n\|_0^2 - \|2v^n - v^{n-1}\|_0^2 + 4\Delta t\,\bar{m}(|u^{n+1}|_1^2 + |u_e^{n+1}|_1^2) \\ &\quad \le \Delta t\,C_1\|u^{n+1}\|_0^2 + \Delta t\,C_2\|v^{n+1}\|_0^2 + \Delta t\,C_3\|u^n\|_0^2 + \Delta t\,C_4\|v^n\|_0^2 \\ &\quad + \Delta t\,C_5\|u^{n-1}\|_0^2 + \Delta t\,C_6\|v^{n-1}\|_0^2 + \Delta t\,C_7\|S^n\|_0^2. \qquad (3.13)\end{aligned}$$

Now sum this inequality for n going from 0 to $m-1$, where m is an integer between 1 and M. We will see the values u^{-1} and v^{-1} appear. They are used during the first time step using the second order SBDF scheme; we will take them equal to u^0 and v^0, respectively. This yields the following result:

$$\begin{aligned}&(1 - \Delta t\,C)\left[\|u^m\|_0^2 + \|v^m\|_0^2\right] + 4\Delta t\,\bar{m}\sum_{n=1}^{m}\left(|u^n|_1^2 + |u_e^n|_1^2\right) \\ &\le 2\left(\|u^0\|_0^2 + \|v^0\|_0^2\right) + \Delta t\,K\sum_{n=0}^{m-1}\left(\|u^n\|_0^2 + \|v^n\|_0^2\right) + \Delta t\,C_7\sum_{n=0}^{m-1}\|S^n\|_0^2, \qquad (3.14)\end{aligned}$$

where $C = \max\{C_1, C_2\}$ and $K = \max\{C_1 + C_3 + 2C_5, C_2 + C_4 + 2C_6\}$. Choose Δt such that $\Delta t < 1/C$, and, by applying the discrete Gronwall lemma to (3.14), obtain

$$\begin{aligned}\max_{n=1,\dots,M}\left\{\|u^n\|_0^2 + \|v^n\|_0^2\right\} \le \Bigg(&\frac{2}{1 - \Delta t\,C}\left[\|u^0\|_0^2 + \|v^0\|_0^2\right] \\ &+ \frac{C_7}{1 - \Delta t\,C}\sum_{n=0}^{M-1}\Delta t\,\|S^n\|_0^2\Bigg)e^{TK/(1-\Delta tC)}. \qquad (3.15)\end{aligned}$$

By combining (3.15) and (3.14), we write

$$\begin{aligned}\sum_{n=1}^{M}\Delta t\left(|u^n|_1^2 + |u_e^n|_1^2\right) \le \frac{1}{2\bar{m}}\left(\|u^0\|_0^2 + \|v^0\|_0^2\right) + \frac{TK}{4\bar{m}}\max_n\left\{\|u^n\|_0^2 + \|v^n\|_0^2\right\} \\ + \frac{C_7}{4\bar{m}}\sum_{n=0}^{M-1}\Delta t\,\|S^n\|_0^2. \qquad (3.16)\end{aligned}$$

This proves that the solutions u, u_e, and v remain bounded in the spaces described in (3.5) for the second order SBDF method, with the condition that $\Delta t < 1/C$ is met. C depends on C_1 and C_2, $C_1 = O(\frac{L_f}{\epsilon})$, and $C_2 = O(\epsilon L_g)$, so we can say that $C = O\left(\max\left\{L_f/\epsilon, \epsilon L_g\right\}\right)$. The stability of the method is guaranteed with $\Delta t = O(\min\{\frac{\epsilon}{L_f}, \frac{1}{\epsilon L_g}\}) = O(\epsilon/L_f)$ when $\epsilon \ll 1$ or $L_f \gg 1$.

3.2.3. Crank–Nicolson/Adams–Bashforth. Take $u^{n+1}+u^n$ and $v^{n+1}+v^n$ as test functions in (2.12) for the Crank–Nicolson/Adams–Bashforth method, and take $\frac{1}{2}(u_e^{n+1}+u_e^n)$ as a test function in (2.2) at times $t=t_n$ and $t=t_{n+1}$. The four resultant equations can then be summed, and by using the Lipschitz condition (3.12) and the equivalence of seminorms we get

$$\begin{aligned}\|u^{n+1}\|_0^2-\|u^n\|_0^2+\|v^{n+1}\|_0^2-\|v^n\|_0^2+\frac{\Delta t}{2}\,\bar{m}(|u^{n+1}+u^n|_1^2+|u_e^{n+1}+u_e^n|_1^2)\\ \le \Delta t\,C_1\|u^{n+1}\|_0^2+\Delta t\,C_2\|v^{n+1}\|_0^2+\Delta t\,C_3\|u^n\|_0^2+\Delta t\,C_4\|v^n\|_0^2\\ +\Delta t\,C_5\|u^{n-1}\|_0^2+\Delta t\,C_6\|v^{n-1}\|_0^2+\Delta t\,C_7\|S^n\|_0^2.\end{aligned}\tag{3.17}$$

By proceeding as we did for the second order SBDF scheme and using the discrete Gronwall lemma,

$$\begin{aligned}\max_{n=1,\dots,M}\left\{\|u^n\|_0^2+\|v^n\|_0^2\right\}\le\Bigg(\frac{1}{1-\Delta t\,C}\left[\|u^0\|_0^2+\|v^0\|_0^2\right]\\ +\frac{C_7}{1-\Delta t\,C}\sum_{n=0}^{M-1}\Delta t\,\|S^n\|_0^2\Bigg)e^{TK/(1-\Delta tC)}\end{aligned}\tag{3.18}$$

and

$$\begin{aligned}\sum_{n=0}^{M-1}\Delta t\big(|u^{n+1}+u^n|_1^2+|u_e^{n+1}+u_e^n|_1^2\big)\le\frac{2}{\bar{m}}\left(\|u^0\|_0^2+\|v^0\|_0^2\right)\\ +\frac{2TK}{\bar{m}}\max_n\left\{\|u^n\|_0^2+\|v^n\|_0^2\right\}+\frac{2C_7}{\bar{m}}\sum_{n=0}^{M-1}\Delta t\,\|S^n\|_0^2,\end{aligned}\tag{3.19}$$

with C and K defined as before and with $\Delta t<1/C$. This time, we need to extend our numerical solutions to functions u, u_e, and v piecewise affine in time, which shows that the solutions u, u_e, and v remain bounded in the spaces in (3.5) with the same conditions as for the second order SBDF scheme.

3.2.4. Forward Euler. The use of explicit methods, such as the forward Euler method considered here, requires more conditions on the time step Δt due to the fact that the diffusion terms are taken explicitly. We use u^{n+1} and v^{n+1} as test functions in (2.12) and u_e^{n+1} in (2.2) at time t_{n+1}, as with the backward Euler and second order SBDF methods, and by adding the resultant variational equations, we get

$$\begin{aligned}\|u^{n+1}\|_0^2+\|u^{n+1}-u^n\|_0^2+\|v^{n+1}\|_0^2+\|v^{n+1}-v^n\|_0^2+2\Delta t\,\bar{m}\left(|u^{n+1}|_1^2+|u_e^{n+1}|_1^2\right)\\ -2\Delta t\,M_i\left[|u^{n+1}-u^n|_1+|u_e^{n+1}-u_e^n|_1\right]|u^{n+1}|_1\\ \le\|u^n\|_0^2+\|v^n\|_0^2+\Delta t\,C_1\|u^{n+1}\|_0^2+\Delta t\,C_2\|v^{n+1}\|_0^2+\Delta t\,C_3\|u^n\|_0^2\\ +\Delta t\,C_4\|v^n\|_0^2+\Delta t\,C_5\|S^n\|_0^2.\end{aligned}\tag{3.20}$$

We must now bound the term with a negative sign in the left-hand side of the previous inequality. Let us rewrite the second variational equation of the system as

$$\begin{aligned}\int_\Omega\left((\sigma_i+\sigma_e)\nabla u_e^{n+1}\right)\cdot\nabla u_e^{n+1}\mathrm{d}\mathbf{x}=-\int_\Omega(\sigma_i\nabla u^{n+1})\cdot\nabla u_e^{n+1}\mathrm{d}\mathbf{x}\\ \Rightarrow|u_e^{n+1}|_1\le\frac{M_i}{m_i+m_e}|u^{n+1}|_1\\ \Rightarrow|u_e^{n+1}-u_e^n|_1\le\frac{M_i}{m_i+m_e}|u^{n+1}-u^n|_1\end{aligned}\tag{3.21}$$

by using the linearity of the second equation of the bidomain model.

By applying an inverse inequality [6, Theorem 3.2.6, p. 140] and the upper bound (3.21) to the inequality (3.20), we obtain the majoration for any constant $s > 0$:

$$\begin{aligned}\|u^{n+1}\|_0^2 + \left(1 - \Delta t \frac{\widetilde{\mathscr{C}}^2 M_i^2 \left(1 + \frac{M_i}{m_i+m_e}\right)^2}{h^2 s}\right) \|u^{n+1} - u^n\|_0^2 + \|v^{n+1}\|_0^2 \\ + \Delta t(2\bar{m} - s)\left(|u^{n+1}|_1^2 + |u_e^{n+1}|_1^2\right) \le \|u^n\|_0^2 + \|v^n\|_0^2 + \Delta t\, C_1 \|u^{n+1}\|_0^2 \\ + \Delta t\, C_2 \|v^{n+1}\|_0^2 + \Delta t\, C_3 \|u^n\|_0^2 + \Delta t\, C_4 \|v^n\|_0^2 + \Delta t\, C_5 \|S^n\|_0^2. \end{aligned} \tag{3.22}$$

To ensure the positivity of all of the terms on the left-hand side of the last inequality, we restrict s and Δt so that $s < 2\bar{m}$ and $1 - \Delta t\, \widetilde{\mathscr{C}}^2 M_i^2 (1 + \frac{M_i}{m_i+m_e})^2 / h^2 s \ge 0$; in other words,

$$\Delta t \le \frac{h^2 s}{\widetilde{\mathscr{C}}^2 M_i^2 \left(1 + \frac{M_i}{m_i+m_e}\right)^2} < \frac{2h^2 \bar{m}}{\widetilde{\mathscr{C}}^2 M_i^2 \left(1 + \frac{M_i}{m_i+m_e}\right)^2}. \tag{3.23}$$

Let $k = 2\bar{m} - s$, $C = \max\{C_1, C_2\}$, and $K = \max\{C_1 + C_3, C_2 + C_4\}$. Proceeding as with the previous methods yields

$$\begin{aligned}\max_{n=1,\dots,M} \left\{\|u^n\|_0^2 + \|v^n\|_0^2\right\} \le \Bigg(\frac{1}{1 - \Delta t\, C}\left[\|u^0\|_0^2 + \|v^0\|_0^2\right] \\ + \frac{C_5}{1 - \Delta t\, C} \sum_{n=0}^{M-1} \Delta t\, \|S^n\|_0^2\Bigg) e^{TK/(1-\Delta t C)}, \end{aligned} \tag{3.24}$$

$$\begin{aligned}\sum_{n=1}^{M} \Delta t \left(|u^n|_1^2 + |u_e^n|_1^2\right) \le \frac{1}{k}\left(\|u^0\|_0^2 + \|v^0\|_0^2\right) + \frac{TK}{k} \max_n \left\{\|u^n\|_0^2 + \|v^n\|_0^2\right\} \\ + \frac{C_5}{k} \sum_{n=0}^{M-1} \Delta t\, \|S^n\|_0^2. \end{aligned} \tag{3.25}$$

Therefore, if the conditions we have imposed on Δt are met, u, u_e, and v remain stable in the spaces of (3.5). These conditions are $\Delta t < 1/C$, with $C = O(\max\{L_f/\epsilon, \epsilon L_g\})$ and the condition (3.23). Clearly Δt must be $O(h^2)$, which limits the applicability of the forward Euler method.

3.2.5. Discussion on the stability conditions. We first want to quantify how small the time step must be to guarantee the stability of fully explicit methods, such as the forward Euler method. We need to estimate the constants in the stability condition (3.23), in particular, $\bar{m}$ and $\widetilde{\mathscr{C}}$.

The last inequality in majoration (3.1) can be rewritten as

$$\begin{aligned} m_i|x+y|^2 + m_e|y|^2 &= m_i|x|^2 + 2m_i\langle x, y\rangle + (m_i + m_e)|y|^2 \\ &= \begin{bmatrix} x & y \end{bmatrix} \begin{bmatrix} m_i & m_i \\ m_i & m_i + m_e \end{bmatrix} \begin{bmatrix} x \\ y \end{bmatrix} \\ &\ge \bar{m}\left(|x|^2 + |y|^2\right), \end{aligned} \tag{3.26}$$

with $\bar{m} > 0$ the smallest eigenvalue of the above matrix. A simple computation gives

$$\bar{m} = \frac{2m_i + m_e - \sqrt{4m_i^2 + m_e^2}}{2} = O(\min\{m_i, m_e\}). \tag{3.27}$$

Let us now estimate the constant $\widetilde{\mathscr{C}}$ that appears in the inverse inequality in [6, Theorem 3.2.6, p. 140]. We will start by evaluating $\widetilde{\mathscr{C}}$ in the 1D case. Consider the function $v_h(x) = a + (b-a)\,x/h \in P_h^1$ on the element $K = [0,h]$. When evaluating $\|v_h\|_0$ and $|v_h|_1$ on K for that function, one must have for the inverse inequality to be valid that:

$$\widetilde{\mathscr{C}} \geq h\frac{|v_h|_1}{\|v_h\|_0} = \left(\frac{3(a-b)^2}{a^2+ab+b^2}\right)^{1/2}. \tag{3.28}$$

It is easy to find that $\widetilde{\mathscr{C}} = 2\sqrt{3}$ is the lowest upper bound for the above rational function.

Now consider the 2D case. Let K be the linear triangular element adjacent to the nodes at $(0,0)$, $(0,h)$, and $(h/2,h/2)$. This is not the most general case, since $\widetilde{\mathscr{C}}$ is likely to depend on the shape of K, but it is nevertheless representative of the meshes we will work with in section 4. Let v_h be a function in P_h^1 on this element with the property that $v_h(0,0) = a$, $v_h(0,h) = b$, and $v_h(h/2,h/2) = c$, i.e., $v_h(x,y) = a + (2c-(a+b))\,x/h + (b-a)\,y/h$. Now let us compute $\|v_h\|_0$ and $|v_h|_1$ on K:

$$\|v_h\|_0 = \left(\int_K v_h^2\,\mathrm{d}\mathbf{x}\right)^{1/2} = \left(\frac{h^2}{24}\left(a^2+b^2+c^2+ab+ac+bc\right)\right)^{1/2}, \tag{3.29}$$

$$|v_h|_1 = \left(\int_K |\nabla v_h|^2\,\mathrm{d}\mathbf{x}\right)^{1/2} = \left(\frac{a^2}{2}+\frac{b^2}{2}+c^2-ac-bc\right)^{1/2}. \tag{3.30}$$

We must choose a value of $\widetilde{\mathscr{C}}$ such that

$$\widetilde{\mathscr{C}} \geq h\frac{|v_h|_1}{\|v_h\|_0} = \left(\frac{12a^2+12b^2+24c^2-24ac-24bc}{a^2+b^2+c^2+ab+ac+bc}\right)^{1/2}. \tag{3.31}$$

In this case, the optimal value for $\widetilde{\mathscr{C}}$ may be computed to be $6\sqrt{2}$.

We consider two cases for the conductivity values.

Case 1: Suppose that $m_i = m_e$ and $M_i = \lambda m_i$ for a certain value $\lambda > 1$. This is in fact a case where the bidomain model reduces to a monodomain model [7, 14]. By using the constants calculated above, the condition on the time step reads as

$$\begin{aligned}\Delta t &< \frac{(3-\sqrt{5})h^2}{\widetilde{\mathscr{C}}^2\lambda^2 m_i\left(1+\lambda+\frac{\lambda^2}{4}\right)}\\ \Rightarrow \Delta t &< \frac{\widetilde{K}h^2}{\lambda^4 m_i} = \frac{\widetilde{K}m_i^3}{M_i^4}h^2,\end{aligned}$$

where $\widetilde{K}$ is a constant that depends on $1/\widetilde{\mathscr{C}}^2$. In that case,

$$\Delta t = O\left(\min\left\{\frac{\epsilon}{L_f}, \frac{1}{\epsilon L_g}, \frac{m_i^3}{M_i^4}h^2\right\}\right).$$

When h becomes small, the last term is the most stringent with a time step that decreases also with the cube of the ratio $m_i/M_i < 1$ of the minimal to maximal intracellular conductivities on the domain.

TABLE 3.1
Stability conditions on Δt and on the model used for several methods.

Method	Δt	Model
Forward Euler	$O\left(\min\left\{\frac{\epsilon}{L_f}, \frac{m_i^3}{M_i^4}h^2\right\}\right)$	f, g Lipschitz
Second order SBDF	$O\left(\frac{\epsilon}{L_f}\right)$	f, g Lipschitz
Backward Euler	$O(\epsilon)$	FitzHugh–Nagumo

Case 2: Take values that approach the physical values found in the heart, for example, those seen in [12], i.e., $m_i = 0.0263$, $m_e = 0.1087$, and $M_i = 0.263$. By substituting these and the constants computed above in (3.23), this would mean in 1D that $\Delta t < 0.00256\,h^2$ and in 2D that $\Delta t < 0.000167\,h^2$. Not only must the maximal time step Δt for stability be in $O(h^2)$, but in practice the constant appearing in that bound is very small. In other words, an explicit method cannot be efficient, especially in higher dimensions or with fine meshes, due to the excessively large number of time steps needed.

Remark 3.2. Suppose that we change the conductivity over the domain while keeping it proportional to what it was before, i.e., replace the conductivity tensors $\sigma_{i,e}$ by $\mu\,\sigma_{i,e}$, just to see how the critical time step scales with the magnitude of the conductivity. Clearly, from condition (3.23), the time step Δt will have to be taken μ times smaller. Therefore increasing the conductivity of the domain will reduce the stability of the forward Euler method.

Table 3.1 summarizes our stability analysis for the numerical time-stepping schemes considered in this section, by supposing that $\epsilon \ll 1$. The stability of implicit and semi-implicit time-stepping schemes is controlled by the time scale of the ion kinetics without regard to the space step size, while for fully explicit methods the space step size also controls the stability through the second order conduction terms.

4. Numerical results. This section presents numerical tests for both 1D and 2D test cases.

4.1. Comparison of the methods in 1D. We have used in the 1D case a simple finite element code written in Matlab. Our linear systems are solved with the LU factorization included in Matlab. The ease of implementation of a 1D code and the ease of use of Matlab have allowed us to test a significant number of methods.

4.1.1. Problem. The 1D bidomain model can be written as

$$\frac{\partial u}{\partial t} = \frac{1}{\epsilon} f(u,v) + \frac{\partial}{\partial x}\left(\sigma_i \frac{\partial u}{\partial x}\right) + \frac{\partial}{\partial x}\left(\sigma_i \frac{\partial u_e}{\partial x}\right), \tag{4.1}$$

$$\frac{\partial}{\partial x}\left(\sigma_i \frac{\partial u}{\partial x}\right) + \frac{\partial}{\partial x}\left((\sigma_i + \sigma_e)\frac{\partial u_e}{\partial x}\right) = 0, \tag{4.2}$$

$$\frac{\partial u}{\partial t} = \epsilon g(u,v), \tag{4.3}$$

where $f(u,v) = u - \frac{u^3}{3} - v$ and $g(u,v) = u + \beta - \gamma v$, with Neumann boundary conditions $\partial_x u(0) = \partial_x u(L) = 0$ and $\partial_x u_e(0) = \partial_x u_e(L) = 0$. Recall that this system determines only u_e modulo a constant. To avoid trying to solve a singular system, we add the condition $u_e(0) = 0$. Our tests have been done over the domain $[0, L]$ with several values of L. We choose as parameter values $\epsilon = 0.1$, $\beta = 1.0$, and $\gamma = 0.5$ and

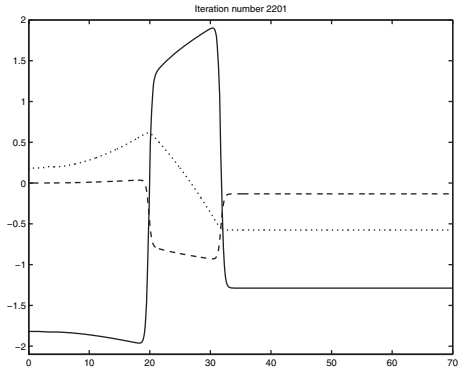

Solid: u; dashed: u_e; dotted: v

FIG. 4.1. *Solution of the* $1D$ *bidomain model's equations at* $t = 11$.

as conductivity tensors $\sigma_i = \sigma_e = 1.0$. Note that all of the parameter values and space and time measures we will use are nondimensional. For the initial condition, we take u and v constant at the equilibrium value of the system $f(u, v) = 0$ and $g(u, v) = 0$ and u_e constant at 0, except on the interval $[0, \frac{1}{20}L]$ where we fix u at a supercritical value, that is, $u(x) = 2$. This creates a traveling pulse wave that propagates through the domain at a constant speed. Figure 4.1 shows a typical wave form at time $t = 11$. Except where specifically mentioned, all tests in this section are done with $L = 70$, and the final time is $T = 30$.

4.1.2. Results. Given the impossibility of obtaining an exact solution to the problem, we have computed a very precise numerical reference solution (mesh resolution $h = 0.007$ and time step $\Delta t = 10^{-4}$) with the second order SBDF scheme (2.14). It is worth noting that, while it is easy to obtain a numerical solution that qualitatively looks like this reference solution, the numerical error may actually be important. The reason is that a space mesh that is too coarse, or a time step that is too large, often produces a traveling wave whose speed is incorrect. Therefore, we consider the relative error between the speed of the reference and numerical solutions as a good measure of the quality of the solution. We will also consider the L^2 error between both solutions.

Table 4.1 shows the value of the critical time step Δt_c, that is, the largest time step for which the solution remains bounded, for several methods and three space resolutions. We have noticed that, for values of Δt slightly inferior to Δt_c, oscillations often appear in regions where the solution has a sharp gradient, but these oscillations remain bounded and do not grow with time. This is probably due to the nonlinear reaction term, and it might be a loss of monotonicity rather than a loss of stability.

As expected from the theoretical stability analysis, the dependence of Δt_c on the mesh resolution varies between the different methods. The forward Euler method's critical time step seems proportional to h^2, in agreement with the analysis in section 3.2.4. By calculating the theoretical critical time steps for that method using the constants obtained in that section and $m_{i,e} = M_{i,e} = 1$, one gets $\Delta t_{c,th} = 5.55 \times 10^{-4}$, 1.39×10^{-4}, and 3.47×10^{-5} for $h = 0.14$, 0.07, and 0.035 ($N = 500$, 1000, and 2000), respectively. The theoretical critical time steps are about 6 times smaller than the experimental critical time steps, but this is not surprising as the theoretical stability conditions obtained above are only sufficient.

TABLE 4.1
Size of Δt_c for the numerical methods used.

Methods	$h = 0.14$	$h = 0.07$	$h = 0.035$
Forward Euler	0.003206	0.000813	0.000204
Forward-backward Euler	0.1395	0.1422	0.1415
Crank–Nicolson	0.1299	0.1044	0.08386
IMEX first order Gear	0.1594	0.1594	0.1594
Backward Euler	> 0.2	> 0.2	> 0.2
CNAB	0.06772	0.04951	0.04027
MCNAB	0.07538	0.075	0.075
Second order SBDF	0.09375	0.09404	0.09494
Implicit Gear	> 0.25	> 0.25	> 0.25
Third order SBDF	0.06834	0.07026	0.07126

For all of the other methods—the implicit, IMEX first order Gear, MCNAB, and second and third order SBDF methods—the critical time step shows limited dependence, if any, on the space step h. The fully implicit methods require the largest Δt_c, followed by the first order IMEX methods and then the higher order IMEX schemes, which require the smallest Δt_c. For the backward Euler scheme, we estimate that $\Delta t_{c,th} \approx 0.04$ by picking the optimal parameter k to equilibrate the leading order terms in $1/\epsilon$ in the stability condition of section 3.2.1. The theoretical step $\Delta t_{c,th}$ is about 5 times smaller than the experimental step Δt_c. Again the theoretical stability condition is only sufficient, which may explain the discrepancy between both values. For fully implicit methods, we have indicated a lower bound for Δt_c because, as Δt gets larger, the nonlinear system is harder to solve with Newton's method, leading to the stagnation of the iterative solver and making an accurate evaluation of Δt_c difficult. Only two semi-implicit methods required smaller Δt_c with smaller space steps h, namely, the CN and CNAB schemes. For those two methods, the dependence of Δt_c on the mesh resolution is at most of sublinear order, unless the asymptotic behavior of Δt_c when h goes to 0 has not yet been reached even with $h = 0.035$.

Figure 4.2 shows the position of the u wave at different times for different methods. The two top figures show the position of the waves at time $t = 20$ computed with all first order methods compared to the position of the reference solution. The bottom figure at the right shows the same thing but for second order methods. For second order methods, we used a time step twice as large as for first order methods to have a comparable workload at each time step and globally to reach a solution at a given time t. Clearly, for a comparable computational effort, second order methods offer greater accuracy with less phase lag compared to the reference solution. The figure at the bottom left shows the solutions obtained with the same second order methods at an earlier time. The phase error between the reference and numerical solution grows with time, as a result of the different wave speeds for the different time integration schemes. We will thus use the wave speed as a measure of error.

Table 4.2 shows the signed relative error between the speed of the numerical wave c_{num} and a reference value c_{ref}, where c_{num} is defined as the average speed at which the level curve for $u = 1$ moves on the interval $[25, 50]$. We have computed the traveling wave speed for our reference solution to be $c_{ref} = 2.577444$. For the section of Table 4.2 dealing with the forward Euler method, we have chosen to show the wave speed for a number of time steps nt approximately equal to the number of time steps necessary to ensure the stability and monotonicity of the solution, as well as for 1.5 and 2 times that number of time steps. For all of the other methods, we could use

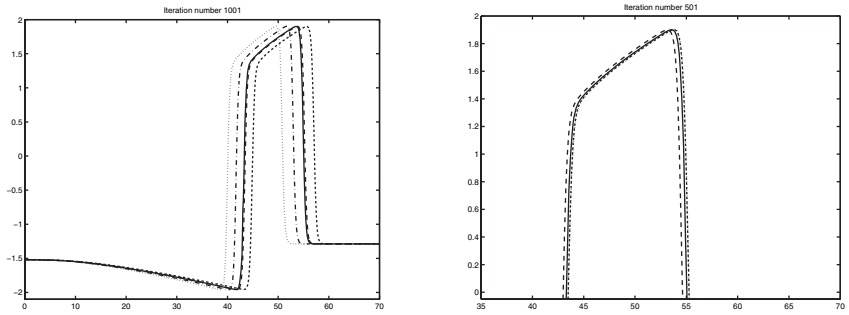

$t = 20$ $t = 20$, zoom

Solid: reference solution
Dashed: CNAB ($\Delta t = 0.02$)
Dash-dot: Crank–Nicolson ($\Delta t = 0.02$)
Dotted: IMEX Gear ($\Delta t = 0.02$)
Short-dashed: Backward Euler ($\Delta t = 0.02$)
Dashed: CNAB ($\Delta t = 0.04$)
Dotted: Implicit Gear ($\Delta t = 0.08$)
Short-dashed: Forward Euler ($\Delta t = 0.0025$)

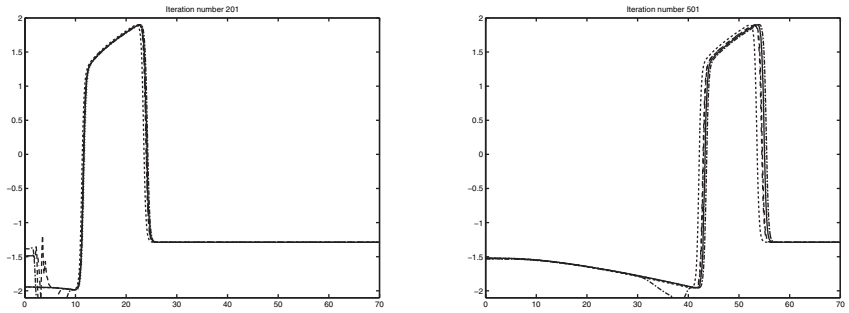

$t = 8$ $t = 20$

Solid: reference solution
Dashed: CNAB ($\Delta t = 0.04$)
Dash-dot: MCNAB ($\Delta t = 0.04$)
Short-dashed: 2^{nd} order SBDF ($\Delta t = 0.04$)
Dash-dash: 3^{rd} order SBDF ($\Delta t = 0.04$)
Dotted: Implicit Gear ($\Delta t = 0.08$)

FIG. 4.2. *Position of the u wave at different t for several methods ($h = 0.14$).*

the same standardized time steps, sufficiently small to ensure the stability of all of the methods.

Table 4.2 clearly shows that with an underresolved grid one cannot reliably compute waves with the right speed, irrespective of the time integration scheme used. It is only for grids with $h \leq 0.14$ that the wave speed error is below 1 %, at least for higher order methods. It had already been observed in [5] that, with a second order fully implicit Gear scheme, 2D action potential waves could travel with the wrong speed due to underresolved spatial grids. Here we emphasize that the grid resolution is only one aspect of the problem; the order of the time integration scheme matters. Finer grids give better accuracy with all methods, but the semi-implicit or implicit first order schemes (Crank–Nicolson, IMEX Gear, and forward-backward Euler in the table) can hardly provide a wave speed error below 1% even on the finest grids considered. It is only by reducing the time step to values comparable to what is used for the forward Euler method that these first order schemes can provide accurate results, at the price of a much higher workload to reach a solution at a given time than for second order methods. Indeed the forward Euler scheme gave the most accurate wave

TABLE 4.2
Relative error (%) between c_{ref} and c_{num}.

Crank–Nicolson/Adams–Bashforth					
	$h = 0.7$	$h = 0.35$	$h = 0.14$	$h = 0.07$	$h = 0.035$
$\Delta t = 0.04$	9.702	1.567	−1.041	−1.591	−1.605
$\Delta t = 0.02$	10.43	2.406	−0.02937	−0.1765	−0.3810
$\Delta t = 0.01$	10.43	2.512	0.07294	−0.07387	−0.07387
$\Delta t = 0.005$	10.36	2.512	0.1242	−0.02250	−0.07387

Modified Crank–Nicolson/Adams–Bashforth					
	$h = 0.7$	$h = 0.35$	$h = 0.14$	$h = 0.07$	$h = 0.035$
$\Delta t = 0.04$	9.702	1.152	−1.440	−1.866	−1.866
$\Delta t = 0.02$	10.43	2.195	−0.02937	−0.3810	−0.4553
$\Delta t = 0.01$	10.43	2.512	0.07294	−0.07387	−0.07387
$\Delta t = 0.005$	10.43	2.565	0.1242	−0.02250	−0.07387

Second order SBDF					
	$h = 0.7$	$h = 0.35$	$h = 0.14$	$h = 0.07$	$h = 0.035$
$\Delta t = 0.04$	8.284	−0.4727	−3.005	−3.544	−3.544
$\Delta t = 0.02$	9.942	1.985	−0.6389	−0.7876	−0.7876
$\Delta t = 0.01$	10.30	2.406	−0.02937	−0.1765	−0.1765
$\Delta t = 0.005$	10.43	2.565	0.1242	−0.07387	−0.07387

Third order SBDF					
	$h = 0.7$	$h = 0.35$	$h = 0.14$	$h = 0.07$	$h = 0.035$
$\Delta t = 0.04$	11.16	3.260	1.003	0.1617	0.1617
$\Delta t = 0.02$	10.67	2.831	0.3812	0.02890	0.09517
$\Delta t = 0.01$	10.55	2.618	0.1755	0.02890	0.02890
$\Delta t = 0.005$	10.43	2.565	0.1755	−0.02250	−0.02250

Crank–Nicolson					
	$h = 0.7$	$h = 0.35$	$h = 0.14$	$h = 0.07$	$h = 0.035$
$\Delta t = 0.04$	2.121	−6.128	−8.454	−8.620	−8.748
$\Delta t = 0.02$	5.999	−1.852	−4.146	−4.491	−4.491
$\Delta t = 0.01$	8.167	0.2318	−2.131	−2.283	−2.381
$\Delta t = 0.005$	9.225	1.411	−0.9911	−1.241	−1.241

IMEX Gear					
	$h = 0.7$	$h = 0.35$	$h = 0.14$	$h = 0.07$	$h = 0.035$
$\Delta t = 0.04$	−5.201	−13.35	−15.13	−15.54	−15.54
$\Delta t = 0.02$	1.708	−6.305	−8.454	−8.620	−8.620
$\Delta t = 0.01$	5.776	−2.046	−4.520	−4.678	−4.678
$\Delta t = 0.005$	7.993	0.1811	−2.229	−2.430	−2.430

Forward-backward Euler					
	$h = 0.7$	$h = 0.35$	$h = 0.14$	$h = 0.07$	$h = 0.035$
$\Delta t = 0.04$	−1.483	−8.889	−11.12	−10.96	−11.21
$\Delta t = 0.02$	4.240	−3.571	−5.808	−5.969	−6.100
$\Delta t = 0.01$	7.243	−0.6721	−3.005	−3.159	−3.159
$\Delta t = 0.005$	8.752	0.8949	−1.490	−1.690	−1.690

Forward Euler					
	$h = 0.7$	$h = 0.35$	$h = 0.14$	$h = 0.07$	$h = 0.035$
nt	770	1900	10000	37300	148000
Δt	0.0390	0.0158	0.003	0.000804	0.000203
% (nt)	−0.03216	0.2905	−0.3046	−0.2089	−0.1023
% $(1.5\,nt)$	1.542	0.8274	−0.1723	−0.1704	−0.09331
% $(2\,nt)$	2.348	1.179	−0.09067	−0.1471	−0.08881

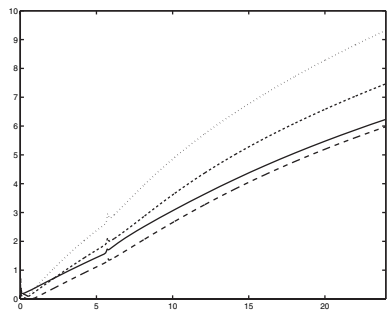

Dotted: IMEX Gear ($\Delta t = 0.02$)
Short-dashed: Forward-Backward Euler ($\Delta t = 0.02$)
Solid: Backward Euler ($\Delta t = 0.02$)
Dashed: Crank–Nicolson ($\Delta t = 0.02$)

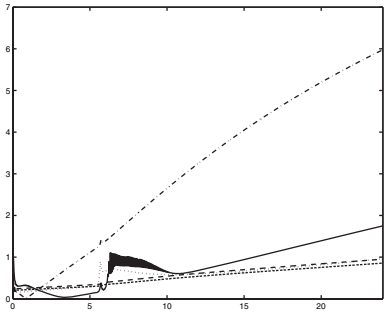

Dash-dot: Crank–Nicolson ($\Delta t = 0.02$)
Solid: CNAB ($\Delta t = 0.04$)
Dashed: CNAB ($\Delta t = 0.02$)
Dotted: Implicit Gear ($\Delta t = 0.08$)
Short-dashed: Forward Euler ($\Delta t = 0.0025$)

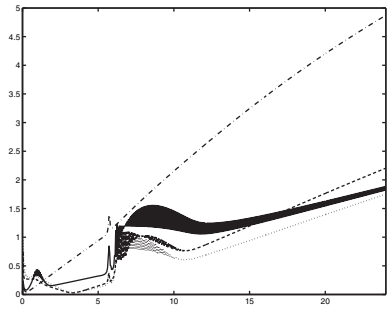

Dotted: CNAB ($\Delta t = 0.04$)
Dashed: MCNAB ($\Delta t = 0.04$)
Dash-dot: 2^{nd} order SBDF ($\Delta t = 0.04$)
Solid: 3^{rd} order SBDF ($\Delta t = 0.04$)

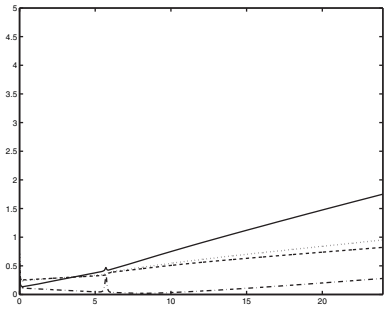

Dotted: CNAB ($\Delta t = 0.02$)
Dashed: MCNAB ($\Delta t = 0.02$)
Dash-dot: 2^{nd} order SBDF ($\Delta t = 0.02$)
Solid: 3^{rd} order SBDF ($\Delta t = 0.02$)

FIG. 4.3. *Evolution in time of the L^2 error for several methods ($h = 0.14$).*

speed on coarse grids and nearly as accurate results as second order schemes on fine grids, but this was done with a prohibitive number of time steps.

Except for circumstantial very accurate results (as with CNAB using $h = 0.07$ and $\Delta t = 0.005$), the most accurate wave speeds have been obtained with the third order SBDF scheme on fine enough grids. It is worth noting, however, that using methods of third order and over isn't necessarily an advantage. The effort in implementing a third order scheme is larger for a marginal gain in accuracy compared to second order schemes. The third order SBDF scheme was also subject to much more stringent numerical stability conditions than its companion second order scheme (see Table 4.1), and even when using a time step size below Δt_c the third order SBDF scheme was more subject to numerical artifacts (Figure 4.2, bottom right). We will come back to this point below when recommending methods.

Finally, Figure 4.3 shows the progression in time of the L^2 error between the reference and numerical solutions for $h = 0.14$. The top two images compare the first order methods to each other and to the second order methods. The two bottom images compare the second and third order methods for two values of Δt. We see that, after a certain time interval in which the action potential wave takes form, the L^2 error then seems to grow linearly in time, although with different slopes for different methods. Among the first order methods, the Crank–Nicolson scheme is the

most accurate. Figure 4.3 confirms the conclusion reached with Table 4.2 that higher order methods are necessary to solve this problem. The error is consistently lower with higher order than first order methods, except for the forward Euler method, which produces results with a L^2 error about the size of the CNAB and implicit Gear schemes but with a much smaller time step than for these second order methods.

Looking back at Figure 4.2 at the bottom, small oscillations are observed in the recovery zone behind the repolarization front for the third order SBDF method. Note that these oscillations are also seen with the CNAB and MCNAB schemes, but they get smoothed out with the advance of time. The third order SBDF scheme gives a bounded solution, but more work must be done to make the instabilities disappear. This method, in fact, does not give better results when $h = 0.14$, as illustrated in Figure 4.3. We may therefore conclude that second order methods are in fact the optimal choice. Among these, we will concentrate on the IMEX schemes, due to the large cost of every time step with the implicit Gear scheme. The second order SBDF method appears to be the most interesting one. As seen in Table 4.1, it is more stable than the CNAB and MCNAB methods—which in fact produce very similar solutions. While it is true (see Figure 4.2 and Table 4.2) that for larger time steps (for example, $\Delta t = 0.04$) the second order SBDF does not preserve the wave speed quite as well as the other two, when smaller time steps are used, it produces an as-good solution. This method also has the advantage of requiring the computation of the diffusion term only at time step $n+1$. For all of these reasons, the second order SBDF method is recommended for solving the bidomain model.

4.2. Comparison of the methods in 2D. In order to solve the 2D bidomain model, we have used an object-oriented finite element code written in C++ based on the solver library PETSc [27]. This library allows the user to choose between many direct and iterative solvers and between many preconditioners. The tests we did on coarse grids have convinced us that the LU factorization is ideal for this problem, subject to memory constraints. When finer grids are used, iterative methods become necessary. Our tests have shown that, of all available solvers and preconditioners, the conjugate gradient method with an incomplete LU preconditioner (see [24]) use the least computation time. The tests shown in this section have been done with this solver and the incomplete LU preconditioner with two levels of fill.

4.2.1. Problem. We consider the 2D formulation of the bidomain model, including Neumann boundary conditions. The domain $[0, 70] \times [0, 70]$ is used—these values again being nondimensional. It is meshed with $4N^2$ triangular elements obtained by dividing the $N \times N$ squares into four congruent triangles. For all of our tests, $N = 300$ ($h = 0.233$). As in the 1D case, we fix the parameters $\epsilon = 0.1$, $\beta = 1.0$, and $\gamma = 0.5$. The degeneracy of the system is removed by fixing the value of u_e somewhere on the domain; we have chosen $u_e(0, 0) = 0$.

The initial condition used in all comparisons done below is obtained numerically as follows. We initiate a spiral (reentrant) wave by setting u and v at their equilibrium value and $u_e = 0$, except on $[0, 3.5] \times [0, 70]$, where we fix $u = 2$ as explained in section 4.1.1, and also on $[31, 39] \times [0, 35]$, where we fix $v = 2$, which creates a recovery zone. The result is a planar wave that travels at constant speed until hitting the recovery zone and then rolls around this zone, forming a spiral wave. Figure 4.4 illustrates the way this spiral wave is formed for the variable u. That spiral wave is then evolved during enough time steps to go through a transient initial stage and reach an established (unsteady) regime. The solution at a given time in that established regime is used as an initial condition. The initial condition is shown on Figure 4.5.

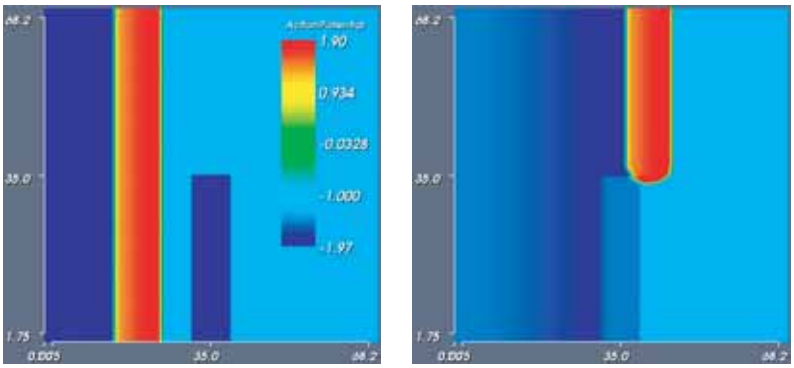

$t = 10$ $t = 20$

$t = 30$ $t = 40$

FIG. 4.4. *Solution for u of the 2D bidomain equations at different times.*

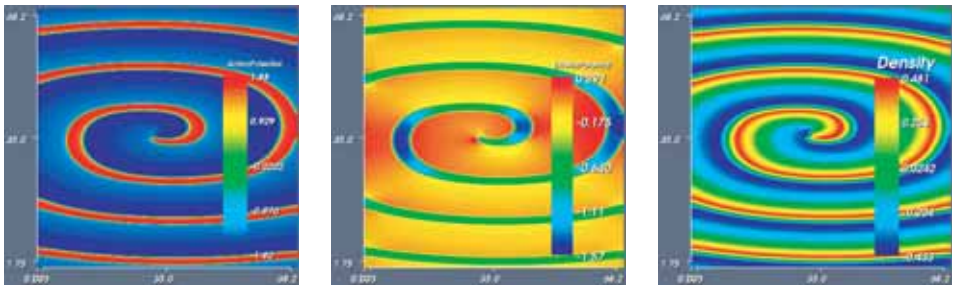

u u_e v

FIG. 4.5. *Initial condition for the 2D problem.*

Due to time and memory constraints, it is very difficult to obtain a precise reference solution in 2D, as was done with 10,000 grid points in 1D. Instead of increasing the number of grid points to a very large value in each direction to reach the grid independence of the numerical solution, we chose to use only $N = 300$ but pick values of the conductivity tensors that are large enough to avoid mesh effects by ensuring a thick enough de-/repolarization wave front. The conductivity tensors are thus taken as $\sigma_i = 25\,\mathrm{diag}\{0.263, 0.0263\}$ and $\sigma_e = 25\,\mathrm{diag}\{0.263, 0.1087\}$. These tensors

TABLE 4.3
Vectors used by different numerical schemes.

	Time derivative		Reaction term		Diffusion term
	t_n	t_{n-1}	t_n	t_{n-1}	t_n
CNAB	X		X	X	X
SBDF2	X	X	X	X	
CN	X		X		X

are proportional to the values suggested by Hooks et al. [12] for the human heart conductivities.

4.2.2. Results. We compare the second order SBDF and the CNAB methods, given the good results they gave in the 1D tests, as well as the Crank–Nicolson–forward Euler method. We use as a comparison point between the different methods the trajectory of the spiral tip. The spiral tip is defined as the point where the level curves with value 0 for u and v meet. We will check if the form of the trajectory of the spiral tip is the same for the numerical solutions and for the reference solution and if there is a drift of the spiral tip.

To speed up computations at each time step, we compute and store the linear system and preconditioner matrices before the first time step and leave them unchanged afterwards. Note that we solve all three equations of the system simultaneously, resulting in matrices with $3 \times 4N^2$ rows for the grid used. These matrices involve the submatrices M, A_i, and A_e defined in section 2.1. Another strategy to reduce the memory requirements would be to solve each equation of the bidomain model separately and do subiterations to solve the coupled linear system at each time step.

The three methods that we have tested require only the two matrices mentioned above. However, they differ in the number of vectors that need assembling at each time step. Table 4.3 shows which vectors are used by each of these three schemes. We suppose that the next time step is the one that will compute the solution at time t_{n+1}. This table shows that the second order SBDF method forces an extra vector—the solution at time t_{n-1}—to be kept in memory but also approximates the diffusion term only at time t_{n+1}, which is included in the linear system matrix, while the other methods require computing the diffusion term at time t_n, needing reassembly at each time step. The assembly of the right-hand term is therefore more costly in terms of computation time for the Crank–Nicolson/Adams–Bashforth and Crank–Nicolson–forward Euler methods than for the second order SBDF method.

We have tested each second order method with three different time steps: $\Delta t = \frac{1}{50}$, $\Delta t = \frac{1}{30}$, and Δt near Δt_c. The Crank–Nicolson method has been tested only with $\Delta t = \frac{1}{50}$ and $\Delta t = \frac{1}{30}$. We have found our values of Δt close to Δt_c with tests with decreasing values of Δt until the method becomes stable. We are thus able to say that, for the initial solution shown in Figure 4.5, $\frac{1}{12} > \Delta t_c \geq \frac{1}{14}$ for the second order SBDF method and $\frac{1}{17} > \Delta t_c \geq \frac{1}{18}$ for the CNAB method. We therefore choose $\Delta t = \frac{1}{18}$ with CNAB and $\Delta t = \frac{1}{14}$ with SBDF. We notice that, just as in the 1D case (see Table 4.1), the SBDF method is slightly more stable than the CNAB method.

We first note that our largest values of Δt are not sufficient to ensure that the solution does not contain oscillations. This is obvious on the third image at the right on the first two lines of Figure 4.6. We already noticed in 1D that the potential wave lags behind when Δt is too large, for both the second order SBDF and CNAB methods (see Table 4.2). We can see in Figure 4.6 that this property remains true in 2D: the solutions for the largest values of Δt do not seem as advanced as for smaller Δt. We

2^{nd} order SBDF method

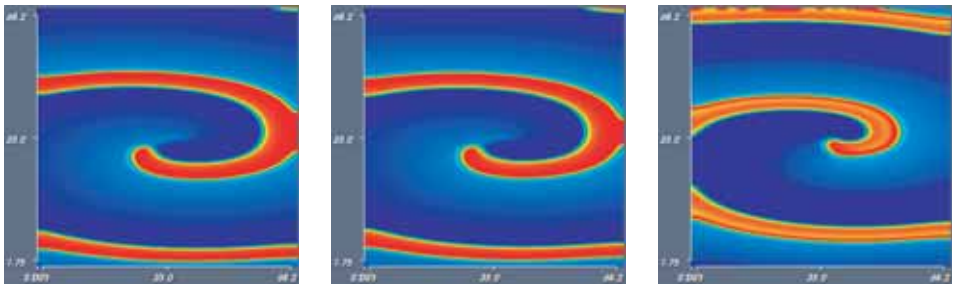

$\Delta t = \frac{1}{50}$ $\Delta t = \frac{1}{30}$ $\Delta t = \frac{1}{14}$

Crank–Nicolson/Adams–Bashforth method

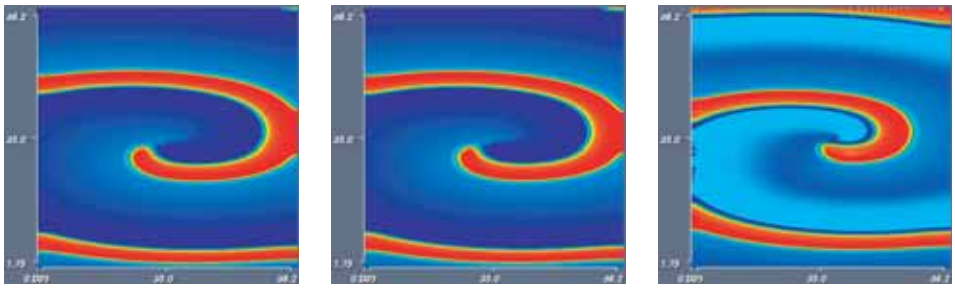

$\Delta t = \frac{1}{50}$ $\Delta t = \frac{1}{30}$ $\Delta t = \frac{1}{18}$

Crank–Nicolson–Forward Euler method

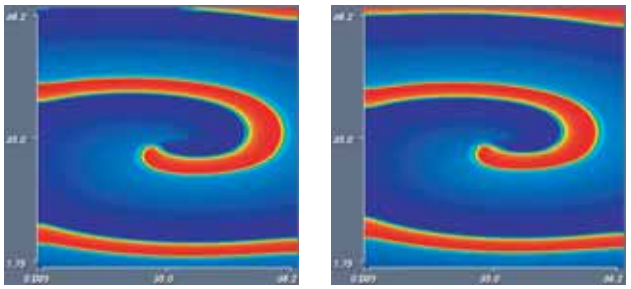

$\Delta t = \frac{1}{50}$ $\Delta t = \frac{1}{30}$

FIG. 4.6. *Solution for u at $t = 80$ with several methods. The legend is the same as for Figure* 4.5.

also remark that the spiral tip drift is very important when Δt is too large, as shown in Figure 4.7(a). The dashed and short-dashed curves, respectively, CNAB with $\Delta t = \frac{1}{18}$ and SBDF2 with $\Delta t = \frac{1}{14}$, get further and further from the solid curve (CNAB with $\Delta t = \frac{1}{50}$) as the solution advances in time. The foot of the trajectory is found at the left in Figures 4.7(a)–(c), while for Figure 4.7(d) it is in the upper right corner.

As in the 1D case, we have been able to determine that first order methods such as the Crank–Nicolson–forward Euler method (2.9) are not really appropriate to solve this particular problem. Even when $\Delta t = \frac{1}{50}$, as seen in the first image of the third

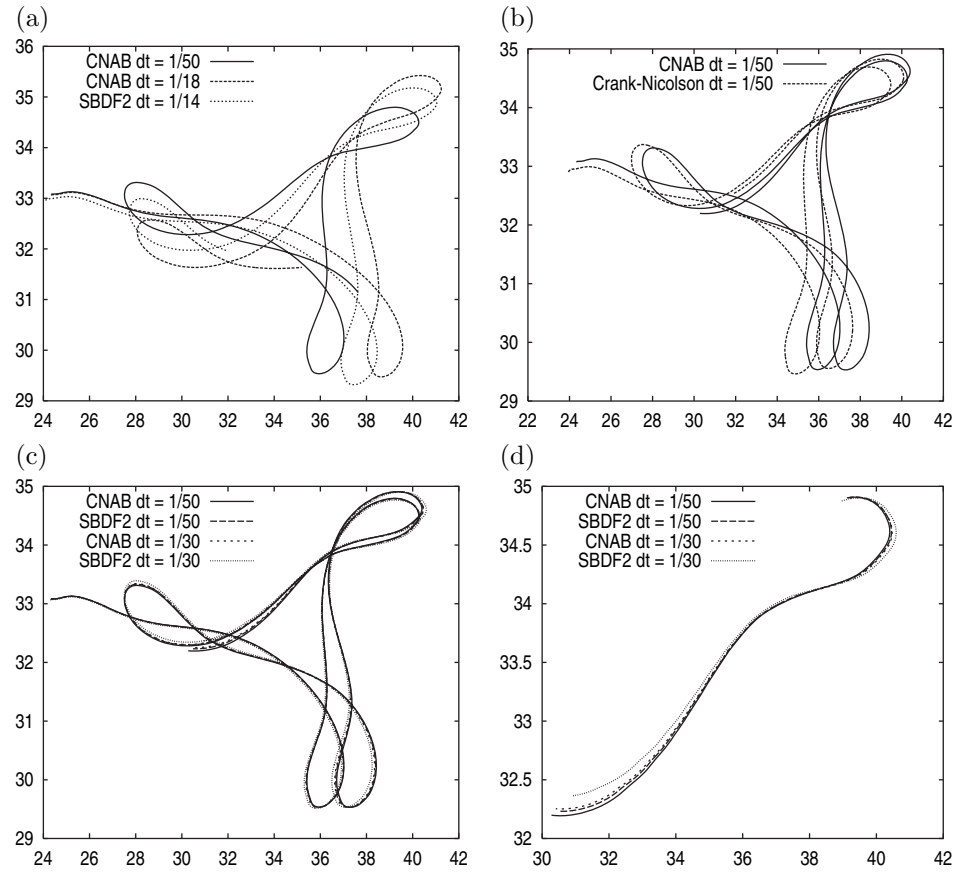

FIG. 4.7. *Trajectory of the spiral tip for:* (a) *second order methods and different values of* Δt, $t \in [10, 55]$*;* (b) *CNAB and CN for* $\Delta t = 1/50$, $t \in [10, 80]$*;* (c) *second order methods and different values of* Δt, $t \in [10, 80]$*;* (d) *second order methods and different values of* Δt, $t \in [70, 80]$.

row of Figure 4.6, the solution already shows an important phase error when compared with the second order methods with $\Delta t = \frac{1}{50}$ or even $\frac{1}{30}$. The error is also visible in Figure 4.7(b), which shows the trajectory of the spiral tip for Crank–Nicolson and CNAB with $\Delta t = \frac{1}{50}$. The error on the spiral tip has already shown up in the 10 time units preceding this image and then increases rapidly.

Figures 4.7(c)–(d) show the evolution of the spiral tip for both second order methods tested, with $\Delta t = \frac{1}{50}$ and $\Delta t = \frac{1}{30}$. The solutions are quite similar regardless of which method is used, but we can note that the solution obtained with the second order SBDF method with $\Delta t = \frac{1}{30}$ drifts slightly compared with the other more accurate results. This fact is more easily seen in Figure 4.7(d). On the other hand, the solution obtained with the CNAB method and $\Delta t = \frac{1}{30}$ follows very closely the more accurate solutions obtained with $\Delta t = \frac{1}{50}$. We recall that in our 1D tests the second order SBDF method produced a wave slightly lagging behind, while the wave computed with the CNAB method was more precisely located for larger values of Δt. Each time step is significantly more costly when solving the 2D problem than the 1D problem, so it is a good idea to use a method that tolerates larger values of Δt. Therefore, the Crank–Nicolson/Adams–Bashforth method seems a more optimal

choice when compared with the second order SBDF method. That being said, the second order SBDF method is almost as accurate as the CNAB method and presents the advantage, as already stated, that each time step is less costly than with the CNAB method, and it is likely that, just as it was with our 1D results, with values of Δt of the order of $\frac{1}{50}$ or less, the second order SBDF method would produce a better solution.

5. Conclusion. In this paper, we have proposed and studied several implicit, explicit, and IMEX time-stepping methods to solve the bidomain model. We have noted that the critical time steps for stability obtained through numerical tests, as seen in Table 4.1, are consistent with the stability analysis of section 3. Indeed, the numerical value of Δt_c depends on h^2 for the forward Euler method, while it has little or no dependence on h for the IMEX and implicit methods. We reached the conclusion that higher order IMEX methods are the most appropriate for solving the bidomain model. Indeed, they are quite stable, their stability does not depend on h, and they produce a good numerical solution even when the time step Δt is not so small. As shown with our numerical results in section 4.1.2, first order schemes, such as the Euler or the Crank–Nicolson methods commonly used for the bidomain model, provide the required accuracy only at the expense of very small time steps, while the second order schemes studied easily provided an error (well) below 1% on the wave speed. It is certainly one of the main conclusions of our work: a second order time-stepping scheme is required, and the Crank–Nicolson scheme the way it is usually implemented for the bidomain model with a fully explicit occurrence of the reaction term does not provide second order accuracy.

Another main advantage of these IMEX methods is that they also require only the solution of a linear system of equations, with both the system and preconditioner matrices constant over the time steps. Second order fully implicit methods are available and slightly more stable, but the matrices involved must be reassembled and factored during Newton–Raphson iterations at each time step.

We have also been able to discriminate between the higher order IMEX methods considered. Two of them have been especially impressive: the CNAB method and the second order SBDF method. We reached the conclusion that, while the SBDF method is more stable than the CNAB method, both methods require a time step about half of its critical value to produce an acceptable solution. With such a value of Δt, the SBDF method produces a solution whose delay compared to the reference solution is slightly larger than the solution obtained with the CNAB method. With yet smaller values of Δt the SBDF method does produce solutions closer to the reference solution than the CNAB method. However, the SBDF method also costs less in terms of computation time than the CNAB method, since it does not require reassembling the diffusion term every time step.

REFERENCES

[1] G. Akrivis, M. Crouzeix, and C. Makridakis, *Implicit-explicit multistep finite element methods for nonlinear parabolic problems*, Math. Comp., 67 (1998), pp. 457–477.

[2] U. M. Ascher, S. J. Ruuth, and B. T. R. Wetton, *Implicit-explicit methods for time-dependent partial differential equations*, SIAM J. Numer. Anal., 32 (1995), pp. 797–823.

[3] P. Bochev and R. B. Lehoucq, *On the finite element solution of the pure Neumann problem*, SIAM Rev., 47 (2005), pp. 50–66.

[4] Y. Bourgault, Y. Coudière, and C. Pierre, *Existence and uniqueness of the solution for the bidomain model used in cardiac electrophysiology*, Nonlinear Anal. Real World Appl., to appear.

[5] Y. Bourgault, M. Ethier, and V. G. LeBlanc, *Simulation of electrophysiological waves with an unstructured finite element method*, Math. Model. Numer. Anal., 37 (2003), pp. 649–661.
[6] P. G. Ciarlet, *The Finite Element Method for Elliptic Problems*, Stud. Math. Appl. 4, North–Holland, Amsterdam, 1978.
[7] P. C. Franzone and G. Savaré, *Degenerate evolution systems modeling the cardiac electric field at micro and macroscopic level*, in Progr. Nonlinear Differential Equations Appl., 50, Birkhauser, Boston, Cambridge, MA, 2002, pp. 49–78.
[8] A. Ern and J.-L. Guermond, *Theory and Practice of Finite Elements*, Appl. Math. Sci. 159, Springer-Verlag, New York, 2004.
[9] P. C. Franzone and L. F. Pavarino, *A parallel solver for reaction-diffusion systems in computational electrocardiology*, Math. Models Methods Appl. Sci., 14 (2004), pp. 883–912.
[10] A. Greenbaum, *Iterative Methods for Solving Linear Systems*, SIAM, Philadelphia, 1997.
[11] N. Hooke, C. S. Henriquez, P. Lanzkron, and D. Rose, *Linear algebraic transformations of the bidomain equations: Implications for numerical methods*, Math. Biosci., 120 (1994), pp. 127–145.
[12] D. A. Hooks, K. A. Tomlinson, S. G. Marsden, I. J. LeGrice, B. H. Smaill, A. J. Pullan, and P. J. Hunter, *Cardiac microstructure: Implications for electrical propagation and defibrillation in the heart*, Circulation Res., 91 (2002), pp. 331–338.
[13] J. P. Keener and K. Bogar, *A numerical method for the solution of the bidomain equations in cardiac tissue*, Chaos, 8 (1998), pp. 234–241.
[14] J. Keener and J. Sneyd, *Mathematical Physiology*, Interdiscip. Appl. Math. 8, Springer-Verlag, New York, 1998.
[15] G. T. Lines, M. L. Buist, P. Grottum, A. J. Pullan, J. Sundnes, and A. Tveito, *Mathematical models and numerical methods for the forward problem in cardiac electrophysiology*, Comput. Vis. Sci., 5 (2003), pp. 215–239.
[16] G. T. Lines, P. Grottum, and A. Tveito, *Modeling the electrical activity of the heart: A bidomain model of the ventricles embedded in a torso*, Comput. Vis. Sci., 5 (2003), pp. 195–213.
[17] M. Murillo and X.-C. Cai, *A fully implicit parallel algorithm for simulating the non-linear electrical activity of the heart*, Numer. Linear Algebra Appl., 11 (2004), pp. 261–277.
[18] R. C. Penland, D. M. Harrild, and C. S. Henriquez, *Modeling impulse propagation and extracellular potential distribution in anisotropic cardiac tissue using a finite volume element discretization*, Comput. Vis. Sci., 4 (2002), pp. 215–226.
[19] M. Pennacchio and V. Simoncini, *Efficient algebraic solution of reaction-diffusion systems for the cardiac excitation process*, J. Comput. Appl. Math., 145 (2002), pp. 49–70.
[20] A. Quarteroni, R. Sacco, and F. Saleri, *Numerical Mathematics*, Texts Appl. Math. 37, Springer-Verlag, New York, 2000.
[21] B. J. Roth, *Frequency locking of meandering spiral waves in cardiac tissue*, Phys. Rev. E, 57 (1998), pp. R3735–R3738.
[22] B. J. Roth, *Meandering of spiral waves in anisotropic cardiac tissue*, Phys. D, 150 (2001), pp. 127–136.
[23] S. J. Ruuth, *Implicit-explicit methods for reaction-diffusion problems in pattern formation*, J. Math. Biol., 34 (1995), pp. 148–176.
[24] Y. Saad, *Iterative Methods for Sparse Linear Systems*, available online from http://www-users.cs.umn.edu/∼saad/books.html, 2000.
[25] R. W. D. Santos, G. Plank, S. Bauer, and E. J. Vigmond, *Preconditioning techniques for the bidomain equations*, in Proceedings of the 15th International Conference on Domain Decomposition Methods, Lect. Notes Comput. Sci. Eng. 40, Springer-Verlag, New York, 2003, pp. 571–580.
[26] J. Sundnes, G. T. Lines, and A. Tveito, *An operator splitting method for solving the bidomain equations coupled to a volume conductor model for the torso*, Math. Biosci., 2 (2005), pp. 233–248.
[27] See the documentation at http://www-unix.mcs.anl.gov/petsc/petsc-2/.